Available online at www.sciencedirect.com

ScienceDirect

IFAC PapersOnline CONFERENCE PAPER ARCHIVE

IFAC PapersOnLine 56-2 (2023) 11639–11644

Dynamic model of a tendon-actuated snake robot using the Newton-Euler formulation

Gianluca D'Antuono * **Kristin Y. Pettersen** *
Luca R. Buonocore ** **Jan Tommy Gravdahl** *
Mario Di Castro **
* *Department of Engineering Cybernetics, Norwegian University of Science and Technology (NTNU), Trondheim, Norway*
** *Mechatronics, Robotics & Operation Section, European Organization for Nuclear Research (CERN), Meyrin, Switzerland*

Abstract: Dynamic models are necessary when dealing with robotic applications where requirements of dexterity, manipulability, payload and compliance have to be satisfied at the same time. This work considers a particular design of tendon-actuated snake-like robots in which links are not coupled through mechanical joints but are free to roll between each other under the effect of cable tension forces. The state of the art in modeling these tendon-actuated rolling-joints systems is limited to kinematic and quasi-static models. In order to simultaneously guarantee modeling accuracy and suitability for model-based control, the Newton-Euler (NE) formulation has been adopted, by taking into account the forces and moments generated by cable tensions, links interactions, inertias, and friction between the rolling surfaces.

Keywords: Modeling, dynamic model, tendon-actuated robots, snake robots, rolling-joints.

1. INTRODUCTION

Performing inspection and maintenance in cluttered and unstructured environments represents a challenging problem in applications where humans cannot directly operate, e.g. because of high rates of radiations, or high magnetic fields. At the accelerator complex of the European Organization for Nuclear Research (CERN) these problems are present in most of the experimental areas. Therefore robots and autonomous systems are widely employed with the aim of guarantying operability, reliability and safety of the experimental facilities.

The context in which our work takes place is the Large Hadron Collider (LHC) (Evans, 2007), a particle accelerator contained in a tunnel with a circumference of 27 km, at a depth up to 175 m. Since the conditions in which the LHC operates are highly critical because of the enormous rates of radiations generated, maintenance and inspection tasks during the operation of the machine are conducted by robotic systems tele-operated from the surface.
However, when dealing with unstructured environments characterized by many obstacles, e.g. devices, tubes and cables, the rigid structure of traditional manipulators tends to be the cause of unwanted collisions and makes it impossible to reach narrow and tight spaces.

The goal of our work, therefore, consists in developing a robotic system able to:

- navigate through intricate paths within a radius of 1 m from the robot base;
- be compliant with the surrounding environment in order to avoid damages at other devices in case of accidental collisions;
- carry some small instrumentation at the end-effector, e.g. cameras and/or sensors.

To fulfill these requirements, a snake-like tendon-actuated manipulator will be employed, since: the hyper-redundant nature of snake-like robots allows to assume complex shapes in the workspace; while the tendon-actuation allows to locate all the motors at the base of the robot, guaranteeing a lightweight and compliant robot body.
In order to take advantage of the full potential of these systems, a mathematical model of the dynamics of the manipulator is needed, both for simulation and model-based control purposes.

Snake-like robots are acquiring increasing attentions in fields of application where dexterity and compliance are crucial for the success of the operation. The need to reach places inaccessible by humans and rigid-link robots has encouraged the development of lightweight and dexterous hyper-redundant robots able to adapt their shape to the surrounding environment by exploiting their large number of degrees of freedom (DoF). Tendon-actuated snake robots, in particular, have been widely employed in medical applications (Burgner-Kahrs et al., 2015), where novel design of endoscopes and minimal invasive surgeries tools have adopted this solution to satisfy both dexterity and payload requirements.
One of the most interesting designs is the one developed by Kim et al. (2014). Thanks to rolling joints coupled orthogonally to each other, the neutral-line of the mechanism varies in relation to the bending angle, and therefore the stiffness of the robot can be controlled by tightening or loosening the cables. This solution gives a great understanding of the potential of these systems, since they can modify their stiffness at any time during operation. Lee et al. (2014) derived the kinematic model of this robot, and implemented an Inverse Kinematic (IK) control in the operational space through the pseudo-inverse Jacobian.

10.1016/j.ifacol.2023.10.502

Another system characterized by rolling-joints is the i^2snake, a snake-like endoscope supported with a robotic arm for global positioning and insertion (Berthet-Rayne et al. (2018)). It consists of 13 stainless steel vertebrae arranged orthogonally allowing motion in 3D. Pairs of rolling-joints moving in the same plane are coupled mechanically, resulting in three actuated sections with 2 DOF and 8 stainless steel tendons each. Even in this case, differential kinematics has been calculated, and an IK controller in the Jacobian null-space has been implemented in order to exploit the redundant DOF of the robotic arm.
Besides the medical field, tendon-actuated snake-like robots have been employed even in larger-scale applications. With the aim of inspect and repair aero-engines, Dong et al. (2017) developed a 1270 mm long robot, and derived a static model to estimate the actuation forces needed. However, for the control of the end-effector trajectory an IK controller has been implemented.

The performance required by the CERN application combines requirements of dexterity and compliance, together with manipulability and capability to hold small payloads. The rolling-joints mechanism proposed by Kim et al. (2014) is able to guarantee these dual characteristics by varying the neutral-line of the manipulator through a proper choice of the cable tensions. Our work will, therefore, be focused on this typology of robot design.

Dynamic models of snake-like cable-driven manipulators are still at their early stage, since most of them are operated far from dynamic boundaries and thus kinematic and quasi-static models are sufficient for their purposes.
For such manipulators to be able to be employed in larger-scale application like the CERN one, however, a dynamic model is required in order to enable model-based analysis and control design to achieve the more demanding dynamic performance. Moreover, it will also enable us to develop a *digital twin* that updates its configuration on the basis of the measurement from the real environment.
In this paper, therefore, we will derive the dynamics of a rolling-joints cable-driven robot, taking into account cable tensions, inertias, gravitational force, external loads, friction and interaction forces generated by the contact between the surfaces of the links.
To this end, we will use the NE formulation for two main reasons: firstly, from a computational point of view the resulting model is less expensive compared to other "energy-based" formulations thanks to its recursive nature; but even more importantly for its usefulness in model-based control of tendon-based snake robots, since it directly derives the actuation forces and torques which then can be used directly for motion planning and control.
The resulting algorithm is based on the solution of an optimization problem (OP) in order to derive the optimal cable tensions to execute a desired joint trajectory.

The paper is organized as follows: Section 2 outlines the robot design and its kinematics, that are essentials to understand the main core of the paper in Section 3, that will derive the formulation of the robot dynamics. In Section 4 the results of the model will be evaluated in simulation, and, lastly, in Section 5, the conclusions of the overall study are made and future work is discussed.

2. BACKGROUND

The following section will first introduce the reader to the robot design considered in this work, and the reasons behind this choice will be explained. In order to derive the velocities of the links and the position of the cables in Section 3, the second part of this section will be dedicated to the direct kinematics of this particular robot structure.

2.1 Robot Design

Among the wide variety of designs discussed in the literaure review of Section 1, the rolling-joints snake-like robot developed by Kim et al. (2014) is one of the solutions that can guarantee good performance both in terms of dexterity and payload. Since the rolling-joint mechanism allows to dynamically act on the stiffness of the manipulator through the tensions of the cables, it is possible to obtain a compliant behavior during the motion, and a stiffer one when the desired configuration is reached. The hollow structure of the robot body, moreover, can be employed as a channel to transport tools or other devices from the base to the end-effector.
As in Kim et al. (2014), the saddle-shaped links are coupled orthogonally to each other in order to allow the motion of the system both in the *pan* direction (belonging to $x-y$ plane in Figure 1) and in the *tilt* direction (belonging to the $x-z$ plane).
Looking at Figure 1, the sections of the links have a circular arc profile at the two extremities that can be described by the following parameters: the *radius of curvature* R, the *contact angle* α, and the *height of the link* H.

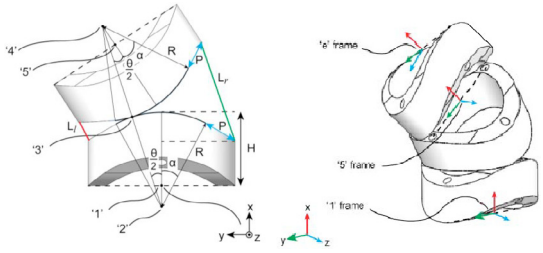

Fig. 1. Kinematics of a 1 DoF (left), and 2 DoF rolling joint (right), Kim et al. (2018)

2.2 Kinematics

Since the kinematics of rolling joints cannot be obtained through the Denavit-Hartenberg convention, Kim et al. (2018) derived the kinematics by looking at the transformation matrices $\mathbf{T}_{f_{j,n}}^{f_{i,n}}$ between intermediate reference frames $f_{i,n}$ and $f_{j,n}$ relative to joint n with $i, j = 1, ..., 5$ and $i \neq j$, and positioned as in Figure 1 (left).

Looking at the kinematics of a 2 DoF rolling joint, reference frames are assigned through the following criteria: the origin is positioned at the center of the link's extremity, the x-axis coincides with the longitudinal axis of the link, the z-axis coincides with the rotation axis around which the rolling motion occurs, while the y-axis is chosen according to the right-hand rule, see Figure 1 (right).

Note: frame $f_{5,n}$ coincides with joint n reference frame.

3. DYNAMIC MODEL

In this section, using the NE formulation, the dynamic model of the tendon-actuated snake robot is developed in a recursive way: in the first step, positions, velocities and accelerations of each link are obtained by evaluating the robot kinematics from the first link to the last link (Section 3.1); the second step consists in deriving the

balance equations of forces and moments acting on each link from last to first (Sections 3.2 and 3.3).

In contrast to the energy-based Lagrange formulation, the NE formulation does not allow for obtaining an analytic expression of the dynamic model in closed-form, but it derives the actuation forces and torques, corresponding to a certain profile of the joints' positions, velocities and accelerations, that satisfy the balance equations previously derived. We will see, however, that, for the robot analyzed in this work, there are infinite combinations of cable tensions that satisfy the balance equations. Therefore, in Section 3.4, an optimization problem will be defined in order to select the optimal cable tensions that satisfy the constraints imposed by the balance equations and the robot mechanics.

3.1 Velocities and Accelerations Propagation

Looking at the 1 DoF joint in Fig. (1), in the whole paper we assume that the links that compose the rolling-joint are constrained to roll without slipping. It is convenient to think about this motion as a pure rotation around the axis passing through the instantaneous contact point (CP) and tangent to the surfaces.

If it is known how one point P on a rigid body is moving, and how the body is rotating, then it is possible to derive the movement of any other point Q on the same body:

$$\mathbf{v}_Q = \mathbf{v}_P + \boldsymbol{\omega} \times \mathbf{d}_{PQ} \ , \tag{1}$$

where $\mathbf{v}_Q$ and $\mathbf{v}_P$ are the linear velocities of points Q and P respectively, $\boldsymbol{\omega}$ is the angular velocity of the rigid body, and $\mathbf{d}_{PQ}$ is the distance vector from P to Q.

Link 1 The angular velocity $\boldsymbol{\omega}_1$ and the angular acceleration $\dot{\boldsymbol{\omega}}_1$ of link 1 rolling on the base link are equal to:

$$\boldsymbol{\omega}_1 = \dot{\theta}_1 \mathbf{z}_0 \ , \tag{2}$$

$$\dot{\boldsymbol{\omega}}_1 = \ddot{\theta}_1 \mathbf{z}_0 + \dot{\theta}_1 \boldsymbol{\omega}_1 \times \mathbf{z}_0 \ . \tag{3}$$

Note that the origin of the instantaneous rotation axis coincides with the origin of the reference frame $f_{3,n}$. Moreover, since the base link is fixed, this point has zero linear velocity, and consequently the linear velocity of the first link frame $\mathbf{v}_1$ can easily be derived by applying (1), with the origin of frame $f_{3,n}$ as point P and the origin of the link frame as point Q:

$$\mathbf{v}_1 = \boldsymbol{\omega}_1 \times \mathbf{d}_{f_{3,1},1} \ , \tag{4}$$

where $\mathbf{d}_{f_{3,1},1}$ represents the distance vector from $f_{3,1}$ to the joint frame, and it can be derived from $\mathbf{T}^{f_{3,1}}_{f_{5,1}}$.

The linear acceleration of link 1, is then:

$$\mathbf{a}_1 = -\mathbf{g}_0 + \dot{\boldsymbol{\omega}}_1 \times \mathbf{d}_{f_{3,1},1} + \boldsymbol{\omega}_1 \times (\boldsymbol{\omega}_1 \times \mathbf{d}_{f_{3,1},1}) \ . \tag{5}$$

Link n For a generic link $n > 1$, the angular velocity $\boldsymbol{\omega}_n$ and acceleration $\dot{\boldsymbol{\omega}}_n$ of the rolling joint n are:

$$\boldsymbol{\omega}_n = \boldsymbol{\omega}_{n-1} + \dot{\theta}_n \mathbf{z}_0 \ , \tag{6}$$

$$\dot{\boldsymbol{\omega}}_n = \dot{\boldsymbol{\omega}}_{n-1} + \ddot{\theta}_n \mathbf{z}_0 + \dot{\theta}_n \boldsymbol{\omega}_n \times \mathbf{z}_0 \ . \tag{7}$$

In this case, frame $f_{3,n}$ has a non-zero linear velocity $\mathbf{v}_{f_{3,n}}$, since link $n-1$ is not fixed.

Following the same arguments as for link 1, the linear velocity of link n is:

$$\mathbf{v}_n = \mathbf{v}_{f_{3,n}} + \boldsymbol{\omega}_n \times \mathbf{d}_{f_{3,n},n} \ . \tag{8}$$

To derive $\mathbf{v}_{f_{3,n}}$, (1) can be employed again, because the velocity of the previous link frame $\mathbf{v}_{n-1}$ has been computed in the preceding step:

$$\mathbf{v}_{f_{3,n}} = \mathbf{v}_{n-1} + \boldsymbol{\omega}_{n-1} \times \mathbf{d}_{n-1,f_{3,n}} \ , \tag{9}$$

where $\mathbf{d}_{n-1,f_{3,n}}$ is the distance vector starting from the origin of link frame $n-1$ and pointing to the origin of frame $f_{3,n}$. Also in this case, $\mathbf{d}_{n-1,f_{3,n}}$ can be derived from the transformation matrix $\mathbf{T}^{n-1}_{f_{3,n}}$.

By substituting (9) into (8), the linear velocity of a generic link frame, $\mathbf{v}_n$, is obtained:

$$\mathbf{v}_n = \mathbf{v}_{n-1} + \boldsymbol{\omega}_{n-1} \times \mathbf{d}_{n-1,f_{3,n}} + \boldsymbol{\omega}_n \times \mathbf{d}_{f_{3,n},n} \ . \tag{10}$$

The acceleration term is the time derivative of (10):

$$\begin{aligned} \dot{\mathbf{v}}_n = \dot{\mathbf{v}}_{n-1} &+ \dot{\boldsymbol{\omega}}_{n-1} \times \mathbf{d}_{n-1,f_{3,n}} + \\ &+ \boldsymbol{\omega}_{n-1} \times (\boldsymbol{\omega}_{n-1} \times \mathbf{d}_{n-1,f_{3,n}}) + \\ &+ \dot{\boldsymbol{\omega}}_n \times \mathbf{d}_{f_{3,n},n} + \boldsymbol{\omega}_n \times (\boldsymbol{\omega}_n \times \mathbf{d}_{f_{3,n},n}) \end{aligned} \ . \tag{11}$$

Center of Mass (CoM) Following the same approach, the velocities and accelerations of the CoM of each link can be calculated. Using the knowledge of the link velocities (10) and replicating the arguments that led to (8), we obtain:

$$\mathbf{v}_{C_n} = \mathbf{v}_n + \boldsymbol{\omega}_n \times \mathbf{d}_{C_n,n} \ . \tag{12}$$

Taking the time derivative of (12), we find that:

$$\mathbf{a}_{C_n} = \dot{\mathbf{v}}_n + \dot{\boldsymbol{\omega}}_n \times \mathbf{d}_{C_n,n} + \boldsymbol{\omega}_n \times (\boldsymbol{\omega}_n \times \mathbf{d}_{C_n,n}) \ , \tag{13}$$

where $\mathbf{d}_{C_n,n} = [-H/2 \ 0 \ 0]^T$, $\forall n = 1, \dots, N$.

3.2 Forces and Moments Propagation

The NE formulation describes the link motion in terms of a balance of forces and moments acting on it. In this section we will present the forces and moments evaluated in the development of the model, and it will be made a distinction between the ones that are due to the cable actuation and the ones generated by links interactions, as done by Rone and Ben-Tzvi (2014) in relation to a tendon-actuated continuum robot with an elastic backbone.

Cable Tension Forces Since the force exerted by a cable has the same direction of the cable itself, the first step to evaluate the tension force is to derive that direction.

According to the robot design presented in Section 2.1, the cables follow a linear path between holes. Consequently, the cable routing along the robot can be derived from the coordinates of the holes $h_{i,n,k}$, where: $i = 1, 2$ distinguishes the holes at the top from the holes at the bottom of each link, respectively, and $k = 1, \dots, 4$ selects the cable. Since the position of the holes wrt the respective link frame can be derived through geometric considerations, cf. Figure 1, the vectors describing the cables $\mathbf{L}_{i,n,k}$ can be deducted as in Rone and Ben-Tzvi (2014):

$$\begin{aligned} \mathbf{L}^n_{1,n,k} &= \mathbf{T}^n_{n-1} \ \mathbf{H}^{n-1}_{2,n-1,k} - \mathbf{H}^n_{1,n,k} \\ \mathbf{L}^n_{2,n,k} &= \mathbf{H}^n_{1,n,k} - \mathbf{H}^n_{2,n,k} \end{aligned} \ , \tag{14}$$

where $\mathbf{H}_{i,n,k}$ is the homogeneous representation of $\mathbf{h}_{i,n,k}$. The unit vectors describing the direction of the cables, $\mathbf{e}_{i,n,k}$, are obtained as:

$$\mathbf{e}_{i,n,k} = \mathbf{L}_{i,n,k} / \|\mathbf{L}_{i,n,k}\| \ . \tag{15}$$

As mentioned before, since tension forces are directed along the cables, they can be expressed as:

$$\mathbf{F}_{T,i,n,k} = F_{T,i,n,k} \ \mathbf{e}_{i,n,k} \ . \tag{16}$$

At each link's cable routing hole, cable tensions generate a force due to their contact with the hole's surface. These contact forces $\mathbf{F}_{con,i,n,k}$ may be determined as follows:

$$\begin{aligned} \mathbf{F}^n_{con,1,n,k} &= \mathbf{F}^n_{T,1,n,k} - \mathbf{F}^n_{T,2,n,k} \ , \\ \mathbf{F}^n_{con,2,n,k} &= \begin{cases} \mathbf{F}^n_{T,2,n,k} & \text{if } n = N \\ \mathbf{F}^n_{T,2,n,k} - \mathbf{F}^n_{T,1,n+1,k} & \text{if } n < N \end{cases} . \end{aligned} \tag{17}$$

Through the computed contact forces, the equivalent actuation forces $\mathbf{F}_{act,n}$ and moments $\mathbf{M}_{act,n}$ relative to the CoM of the link are obtained:

$$\mathbf{F}^n_{act,n} = \sum_k \mathbf{F}^n_{con,1,n,k} + \mathbf{F}^n_{con,2,n,k} \tag{18}$$

$$\begin{aligned}\mathbf{M}^n_{act,n} = &\sum_k (\mathbf{h}^n_{1,n,k} - \mathbf{p}^n_{C_n}) \times \mathbf{F}^n_{con,1,n,k} \\ &+ (\mathbf{h}^n_{2,n,k} - \mathbf{p}^n_{C_n}) \times \mathbf{F}^n_{con,2,n,k}\end{aligned} \tag{19}$$

where $\mathbf{p}^n_{C_n}$ is the position vector of the CoM.
By substituting the values of the cable-hole contact force (17) into (18) and (19), and collecting the terms, we obtain:

$$\mathbf{F}^n_{act,n} = \begin{cases} \sum_k \mathbf{F}^n_{T,1,n,k} & \text{if } n = N \\ \sum_k \mathbf{F}^n_{T,1,n,k} - \mathbf{F}^n_{T,1,n+1,k} & \text{if } n < N \end{cases} \tag{20}$$

$$\mathbf{M}^n_{act,n} = \begin{cases} \sum_k (\mathbf{h}^n_{1,n,k} - \mathbf{p}^n_{C_n}) \times \mathbf{F}^n_{T,1,n,k}\ , & \text{if } n = N \\ \sum_k \big((\mathbf{h}^n_{1,n,k} - \mathbf{p}^n_{C_n}) \times \mathbf{F}^n_{T,1,n,k} + \\ \quad - (\mathbf{h}^n_{2,n,k} - \mathbf{p}^n_{C_n}) \times \mathbf{F}^n_{T,1,n+1,k} \big), & \text{if } n < N \end{cases} \tag{21}$$

where, for (21), we have exploited the fact that $(\mathbf{h}^n_{2,n,k} - \mathbf{h}^n_{1,n,k}) \times \mathbf{F}^n_{T,2,n,k}$ is zero, since the two vectors are parallel.

Link Inertia Following the arguments presented by Siciliano et al. (2010) (Section 7.1), it is convenient to refer the inertia force and moment to the current reference frame, in order to handle a constant inertia tensor $\bar{\mathbf{I}}_n$. As a result, it holds that:

$$\mathbf{F}^n_{in,n} = m_n \dot{\mathbf{v}}_{C_n} \tag{22}$$

$$\mathbf{M}^n_{in,n} = \bar{\mathbf{I}}^n_n \dot{\omega}^n_n + \omega^n_n \times (\bar{\mathbf{I}}^n_n \omega^n_n) \tag{23}$$

Gravitational Load The effect of the gravitational field on each link can be included by initializing the acceleration, i.e. by choosing the initial condition $\mathbf{a}_0$ equal to the gravitational acceleration vector $-\mathbf{a}_g$.

Link Interaction Forces Considering link n, interaction forces are generated from its contact with both its neighboring links, $n+1$ and $n-1$. During the rolling motion of these saddle-shaped links, the contact takes place in two regions of the surfaces of the links. Considering these distributed contacts as concentrated in two points c_i with $i = 1, 2$, the vector $\mathbf{f}_{c_i,n}$ represents the force exerted from link $n-1$ on link n at the contact point c_i.

Friction Force A further component that cannot be disregarded in the balance equations is the friction force $\mathbf{f}_{S,c_i,n}$ generated at the contact points c_i between the surfaces of the links. To highlight the relevance of this force, just consider the simpler case of a single rolling joint as in Figure 1 (left), and assume the gravity force directed towards $-z$ direction. Actuation cables can only exert tensions on the $x-y$ plane, then there is no combination of tension forces to balance the weight of the structure on the z-component. The static friction force is, therefore, the only one able to balance the gravity load in that direction.

The friction force depends on: the static friction coefficient μ_s and the interaction force normal to the surfaces. Since the latter is directly related to the tension forces, it follows that it is possible to act on the friction forces needed to satisfy the balance equations through the cable tensions.

3.3 Balance Equations

Once all the forces acting on a generic link n have been identified, we are ready to formulate the balance equations: *Newton's equation* for the translational motion of the CoM, and *Euler's equation* for the rotational motion.
Hereafter, for the sake of readability, the superscripts will be omitted when the quantity is referred to the current link reference frame.

Link N Recall that during the rolling motion of the saddle-shaped links there are two contact points. The contributions due to link interaction and friction forces are generated in these locations. For this reason, the Newton's Equation assumes the following form:

$$\mathbf{F}_{act,N} + \mathbf{f}_{c_1,N} + \mathbf{f}_{c_2,N} + \mathbf{f}_{S,c_1,N} + \mathbf{f}_{S,c_2,N} = \mathbf{F}_{in,N}\ . \tag{24}$$

Inserting the expression of the actuation force (20), (24) becomes:

$$\sum_k (\mathbf{F}_{T,1,N,k}) + \mathbf{F}_{c_1,N} + \mathbf{F}_{c_2,N} = \mathbf{F}_{in,N}\ , \tag{25}$$

with $\mathbf{F}_{c_i,n} = \mathbf{f}_{c_i,n} + \mathbf{f}_{S,c_i,n}$, for $i = 1, 2$.

The following equation represents the Euler's equation with the moments about the CoM of the link:

$$\begin{aligned}\mathbf{M}_{act,N} + (\mathbf{p}_{c_1,N} - \mathbf{p}_{C_N}) \times \mathbf{F}_{c_1,N} + \\ + (\mathbf{p}_{c_2,N} - \mathbf{p}_{C_N}) \times \mathbf{F}_{c_2,N} = \mathbf{M}_{in,N}\end{aligned} \tag{26}$$

By substituting the moment generated by the cables (21) into (26), we get:

$$\begin{aligned}\sum_k \Big((\mathbf{h}_{1,N,k} - \mathbf{p}_{C_N}) \times \mathbf{F}_{T,1,N,k} \Big) + \\ + (\mathbf{p}_{c_1,N} - \mathbf{p}_{C_N}) \times \mathbf{F}_{c_1,N} + \\ + (\mathbf{p}_{c_2,N} - \mathbf{p}_{C_N}) \times \mathbf{F}_{c_2,N} = \mathbf{M}_{in,N}\end{aligned} \ . \tag{27}$$

Equations (25) and (27) show that the tension force $\mathbf{F}_{T,2,N,k}$ of the cables passing through the link's structure does not play any role in the balance of forces and moments.

Link n Concerning the balance equations of link n, with $1 \le n < N$, it has to be highlighted that, in this case, interaction and friction forces are not only generated from the contact between links n and $n-1$, but also from the contact between links n and $n+1$. For this reason the derivation of the balance equations becomes more cumbersome, although the approach is the same as the one used for link N.

Evaluating again (20) for a generic link n, and collecting the terms that correspond to the inertia forces calculated at the previous steps, Newton's equation becomes:

$$\sum_k (\mathbf{F}_{T,1,n,k}) + \mathbf{F}_{c_1,n} + \mathbf{F}_{c_2,n} = \mathbf{F}_{in,n} + \sum_{j=n+1}^{N} (\mathbf{R}^n_j \mathbf{F}^j_{in,j})\ . \tag{28}$$

Euler's equation for a generic link n is represented by:

$$\begin{aligned}\mathbf{M}_{act,n} + \sum_i \big((\mathbf{p}_{c_i,n} - \mathbf{p}_{C_n}) \times \mathbf{F}_{c_i,n} + \\ - (\mathbf{p}_{c_i,n+1} - \mathbf{p}_{C_n}) \times \mathbf{F}_{c_i,n+1} \big) = \mathbf{M}_{in,n}\end{aligned} \tag{29}$$

Substituting the moment generated by the cables with the right-hand side terms of (21) for $n < N$, gives:

$$\begin{aligned}\sum_k \big((\mathbf{h}_{1,n,k} - \mathbf{p}_{C_n}) \times \mathbf{F}_{T,1,n,k}\big) \; + \\ + \sum_i \big((\mathbf{p}_{c_i,n} - \mathbf{p}_{C_n}) \times \mathbf{F}_{c_i,n}\big) = \\ = \mathbf{M}_{in,n} + \sum_k \big((\mathbf{h}_{2,n,k} - \mathbf{p}_{C_n}) \times \mathbf{F}_{T,1,n+1,k}\big) \; + \\ + \sum_i \big((\mathbf{p}_{c_i,n+1} - \mathbf{p}_{C_n}) \times \mathbf{F}_{c_i,n+1}\big)\end{aligned} \tag{30}$$

3.4 Optimization Problem

As mentioned in the introduction of Section 3, the NE formulation aims to derive the actuation forces that solve the set of balance equations.

In contrast to conventional robots, where each joint is actuated by a motor, in our tendon-actuated robot each section is actuated by 4 cables. In the former case, the actuation torques/forces that solve the set of balance equations is unique; while in the latter case, the combination of cable tensions that solve the set of equations is not unique. The set of equations made by (25), (27), (28) and (30), indeed consists of 6 equations with 16 unknowns, $\mathbf{u}$, i.e. the 3 vectorial components of $\mathbf{f}_{c_1,n}$, $\mathbf{f}_{c_2,n}$, $\mathbf{f}_{S,c_1,n}$, $\mathbf{f}_{S,c_2,n}$, and the magnitudes of the 4 tension forces $\mathbf{F}_{T,1,n,k}$.

To choose between these infinite combinations of cable tensions that satisfy the balance equations, in this section we thus define an optimization problem in order to select the optimal cable tensions to execute a desired trajectory in the joint space. Xu et al. (2018) apply this method for a different rigid-link cable-driven robot, where the presence of universal joints independently actuated allows them to simplify the formulation of the problem to a set of 3 equations in 4 unknowns, considering as constraints the sole set of balance equations. In our case, the rolling-joint structure imposes a different setting of the problem, since the constraints have to reflect the behavior of the system.

The first constraints to be fulfilled are, of course, the balance equations of forces and moments, (25) and (27), or (28) and (30), depending on which link we are considering. Secondly, a minimum tension of the cables has to be guaranteed, i.e. a pretension $\bar{F}_T$, in order to avoid cable slackness during the operation:

$$F_{T,1,n,k} \geq \bar{F}_T \;, \text{ for } k = 1, \dots, 4 \;. \tag{31}$$

A further consideration has to be done about the components of the interaction forces. Looking at Figure 1, if we evaluate the interaction force wrt the link reference frame f_3, the only non-zero component is the one along the x-axis, since it is the axis oriented normally to the surfaces:

$$(\mathbf{f}_{c_i,n}^{f_{3,n}})_y = 0 \;,\; (\mathbf{f}_{c_i,n}^{f_{3,n}})_z = 0 \;. \tag{32}$$

Just like what has been done so far for the links interaction force, even for the friction force there are some considerations to do about its components. The direction of the static friction is always opposed to the body motion and orthogonal to the normal component to the surface. When rolling without slipping, the motion of the instantaneous contact points is always tangent to the surfaces. For this reason, if evaluated wrt the link reference frame $f_{3,n}$, the friction force has a zero component along the x-axis:

$$(\mathbf{f}_{S,c_i,n}^{f_{3,n}})_x = 0 \;. \tag{33}$$

In addition to purely geometric arguments, some considerations have to be made about the bounds on the interaction and friction forces. Since the structure of our robot does not provide a strictly mechanical coupling between links, in order to ensure continuous contact between the two surfaces, a minimum interaction force along the normal direction has to be guaranteed. By our choice of link frames, the unit vector normal to the contact surfaces coincides with the x-axis of the link reference frame $f_{3,n}$. Therefore, this requirement of a minimum interaction force is satisfied if the x-component of the link interaction force wrt $f_{3,n}$ is greater than a threshold value, $\bar{f}_c$, that is:

$$(\mathbf{f}_{c_i,n}^{f_{3,n}})_x \geq \bar{f}_c \;, \text{ for } i = 1, 2 \;. \tag{34}$$

A further subject concerns the contact friction forces $\mathbf{f}_{S,c_i,n}$. With respect to the local reference frame f_3, a pure rolling without sliding motion is guaranteed if and only if the following conditions are satisfied:

$$|(\mathbf{f}_{S,c_i,n})_y^{f_{3,n}}| \leq \mu_s |(\mathbf{f}_{c_i,n}^{f_{3,n}})_x| \;, \tag{35}$$

$$|(\mathbf{f}_{S,c_i,n})_z^{f_{3,n}}| \leq \mu_s |(\mathbf{f}_{c_i,n}^{f_{3,n}})_x| \;. \tag{36}$$

A physical interpretation of constraints (35) and (36) is attributable to the fact that, if the friction force exceeds in magnitude the interaction force, the tangential component is greater than the normal component, therefore the sliding motion will prevail over the rolling one.

Once all the constraints have been set, the objective function must be defined. From a control point of view it is preferable to perform a desired motion with as small cable forces as possible, so we let the optimization routine seek to minimize the sum of the cable tension forces.

Now that we have defined all the factors that we want to take into account, we can compose the OP as follows:

$$\begin{aligned} \min_{\mathbf{u}} \quad & \sum_k \mathbf{F}_{T,1,n,k} \\ \text{s.t.} \quad & (25), (27), (31) - (36) \quad , \text{ if } n = N \\ & (28), (30) - (36) \quad , \text{ if } n < N \end{aligned} \tag{37}$$

3.5 Recursive Algorithm

The structure of the set of balance equations allows the solution of (37) through a recursive algorithm.

Once the profiles of position, velocity and acceleration of each joint, $\boldsymbol{\theta}, \dot{\boldsymbol{\theta}}, \ddot{\boldsymbol{\theta}}$, are given, the recursive algorithm consists of the following steps:

- Through relations (2), (3), (5), (6), (7), (11), (13), with $n = 1, \dots, N$, the quantities $\boldsymbol{\omega}_n^n$, $\dot{\boldsymbol{\omega}}_n^n$, $\mathbf{a}_n^n$, $\mathbf{a}_{C_n}^n$ are calculated;
- for each link $n = N, \dots, 1$, the optimization problem (37) is solved, finally giving the cable tensions to exert at the base, $F_{T,1,0,k}$, with $k = 1, \dots, 4$.

4. SIMULATION STUDY

In this section we present a simulation study to evaluate the response of the algorithm in terms of how the resulting cable tensions behave, given the profiles of position, velocity and acceleration of each joint.

For the sake of simplicity when evaluating the tension plots, the simulation study will be conducted on a single section with 6 rolling joints. Note, however, that the approach described in this work is completely general and can be applied for an arbitrary number of joints and sections. Seeking to emulate a condition similar to the real application at the CERN facility, the robot is assumed to be attached to a vertical wall, as if it were a cantilever beam,

with gravity pointing along the $-\mathbf{z}_0$ axis.

Three simulations have been conducted, by applying the joint trajectory $\theta_n = \frac{\pi}{18}\sin(t/2)$ to joints $n = \{1, 3, 5\}$, $n = \{2, 4, 6\}$, and $n = \{1, ..., 6\}$, respectively. The resulting cable tensions at the base obtained from each simulation (with time step $t_S = 5 \cdot 10^{-3} s$) are shown in Figure 2.

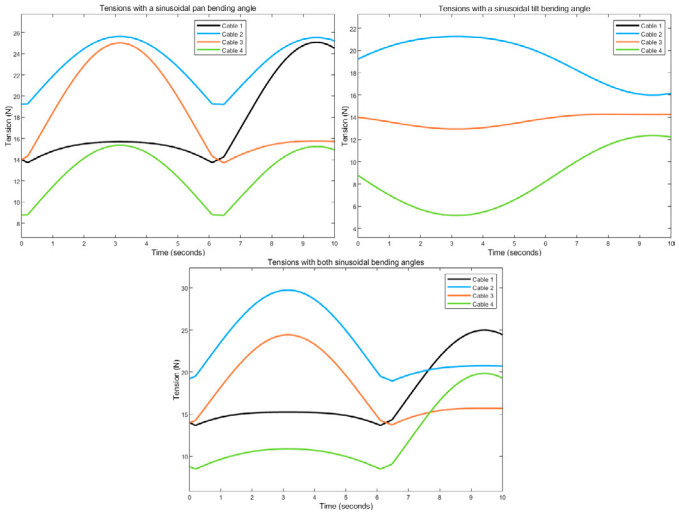

Fig. 2. Cable tensions for a sinusoidal pan (top left), tilt (top right), and 3D (bottom) motion

The first simulation (top left) shows that, even though it is the contraction of cables 1 (black) and 3 (red) that allows the joints to bend in the pan direction, the cable with the highest tension is cable 2 (blue). This behavior is due to the fact that cable 2 is the one located at the bottom side of the robot, and thus it is the cable most affected by the weight of the mechanical structure.

In the second simulation (top right), the greater tension exhibited by cable 2 is due both to the actuation force of the tilt joints, and to the compensation of the gravity load, which are the two forces that prevail over the other ones. The weight force, in particular, is the one that mostly affect the cable tensions. This fact is particularly noticeable looking at the last 3 seconds of the simulation, when the robot is bending towards the ceiling. Even in this case, despite that the tension of cable 4 is at its maximum, it still does not exceed in magnitude the one of cable 2. A further insight to be highlighted about the behavior of the system is the coincidence of the tension forces at the base of cables 1 and 3. This reflects the fact that when the robot bends up and down in the tilt direction, then the forces in the pan direction are equally distributed.

The last simulation scenario (bottom) is a combination of the first two, so the most complex bending shape results in cable tensions of higher magnitude than those of the previous cases, e.g. the peak tension magnitude of cable 2 increases by almost 43% wrt the case in which the pan joints were kept zero. This behavior reflects the fact that, even if the joint trajectories are the same as in the previous cases if considered singularly, the tension of the cables actuating the tilt joints are influenced also by the status of the pan joints and vice versa.

5. CONCLUSIONS

Among the wide variety of dynamics formulations available, the NE formulation turns out to be a suitable choice for snake-like tendon-actuated robots for two main reasons: firstly from a computational point of view, since the resulting model is less computationally expensive compared to other "energy-based" formulations thanks to its recursive nature; and secondly for its usefulness in model-based control, since it directly derives the actuation forces which can be used directly for motion planning and for model-based control, e.g. to compensate for the nonlinear terms that characterize the robot dynamics.
By applying the NE formulation to a novel class of tendon-actuated rolling-joints robot, the components in terms of forces and moments generated by cable actuation, inertias, interaction between links and static friction at the contact points between the rolling surfaces, have been derived. The wide variety of forces and moments considered, gives to this formulation a high relevance even for simulation purposes, e.g. to evaluate the feasibility of a certain trajectory.

5.1 Future Work

The next important step that will be conducted is the validation of the dynamic model, first via Multibody Dynamics simulations, and then by building a prototype. This will make it possible to take into consideration even more complex physical phenomena, like the cable tension loss due to the interaction between the cable and their channel guide when sliding through the links.

REFERENCES

Berthet-Rayne, P., Gras, G., Leibrandt, K., Wisanuvej, P., Schmitz, A., Seneci, C., and Yang, G.Z. (2018). The i²snake robotic platform for endoscopic surgery. *Annals of Biomedical Engineering*, 46.

Burgner-Kahrs, J., Rucker, D.C., and Choset, H. (2015). Continuum robots for medical applications: A survey. *IEEE Trans. Robotics*, 31(6), 1261–1280.

Dong, X., Axinte, D., Palmer, D., Cobos, S., Raffles, M., Rabani, A., and Kell, J. (2017). Development of a slender continuum robotic system for on-wing inspection/repair of gas turbine engines. *Robotics and Computer-Integrated Manufacturing*, 44, 218–229.

Evans, L. (2007). The large hadron collider. *New Journal of Physics*, 9(9), 335.

Kim, K., Woo, H., and Suh, J. (2018). Design and evaluation of a continuum robot with discreted link joints for cardiovascular interventions. In *Proc. 7th IEEE Int. Conf. BioRob*, 627–633.

Kim, Y.J., Cheng, S., Kim, S., and Iagnemma, K. (2014). A stiffness-adjustable hyperredundant manipulator using a variable neutral-line mechanism for minimally invasive surgery. *IEEE Trans. Robotics*, 30(2), 382–395.

Lee, J., Kim, J., Lee, K.K., Hyung, S., Kim, Y.J., Kwon, W., Roh, K., and Choi, J.Y. (2014). Modeling and control of robotic surgical platform for single-port access surgery. In *Proc. IEEE/RSJ Int. Conf. Intelligent Robots and Systems*, 3489–3495.

Rone, W.S. and Ben-Tzvi, P. (2014). Continuum robot dynamics utilizing the principle of virtual power. *IEEE Trans. Robotics*, 30(1), 275–287.

Siciliano, B., Sciavicco, L., Villani, L., and Oriolo, G. (2010). *Robotics: Modelling, Planning and Control*. Springer Publishing Company, Incorporated.

Xu, W., Liu, T., and Li, Y. (2018). Kinematics, dynamics, and control of a cable-driven hyper-redundant manipulator. *IEEE Trans. Mechatronics*, 23(4), 1693–1704.